

Supplemental Information for
**Coseismic and early postseismic deformation in the August 14, 2021 Haiti
earthquake from satellite-based geodesy**

J. Maurer, R. Dutta, A. Vernon, and S. Vajedian

Missouri University of Science and Technology, Geological Sciences and Geological and
Petroleum Engineering, Rolla, MO 65401, United States

Contents

Supplemental Text S1-S2.

Supplemental Figures S1 – S20.

Supplemental Tables S1 – S4.

Supplemental Text S1. Fault database compilation details

The fault map dataset was refined and augmented using several other data sources, including Saint Fleur et al. (2020), Possee et al. (2019), who drew on work from Corbeau et al. (2016b), Conrad et al. (2020), the USGS lithology database (French & Schenk, 2004), and both SRTM and LiDAR DEMs available for Haiti. We compared traces between sources and topography in QGIS to best determine the fault geometry at the surface. We provide an update to the CCAF-DB on Github (https://github.com/jlmaurer/central_am_carib_faults). These traces were then discretized into segments that formed the basis of the fault model (Figure 1 in the main text).

Supplemental Text S2. Plane-strain (2D) fault model to solve for fault dip

We take a profile through ALOS-2 track 43 LOS displacements at 73.67°W (20 km west of the origin in the local coordinate system). The track 43 InSAR observations are the most reliable displacement information that we have in the main area of the rupture, due to the low coherence of the Sentinel-1 InSAR observations, noise in the Sentinel-1 pixel offsets, and a lack of data coverage south of the EPGFZ for track 138. The rupture at this location was primarily dip-slip, and we model it using a plane-strain 2D elastic dislocation and solve for the parameters that explain the observations. We use the Metropolis-Hastings version of Markov-Chain Monte Carlo (MCMC) to find the full posterior distribution on the parameters of the model (slip, depth, fault length and position, and dip) to fit the profile (Figure S20). Best-fitting parameters (maximum likelihood estimate) are: slip = 2.11 m (reverse slip), depth to the top of fault = 5.64 km, fault dip = 52.35 degrees, dipping north, fault length = 22.68 km. x-location of the top of the fault is at 0.40 km north of the origin. Figure S20 shows the MCMC results and best-fitting model.

Supplemental Figures

Figure S1 (next page). Regional seismo-tectonic setting of Hispaniola. Fault lines are modified from Styron et al. (2020), Conrad et al. (2020), and NASA (2020). The earthquakes with magnitude more than 3.5 are obtained from ANSS Comprehensive Earthquake Catalog and USGS earthquake catalog. Gray lines are the locations of the seismicity profiles shown on the right.

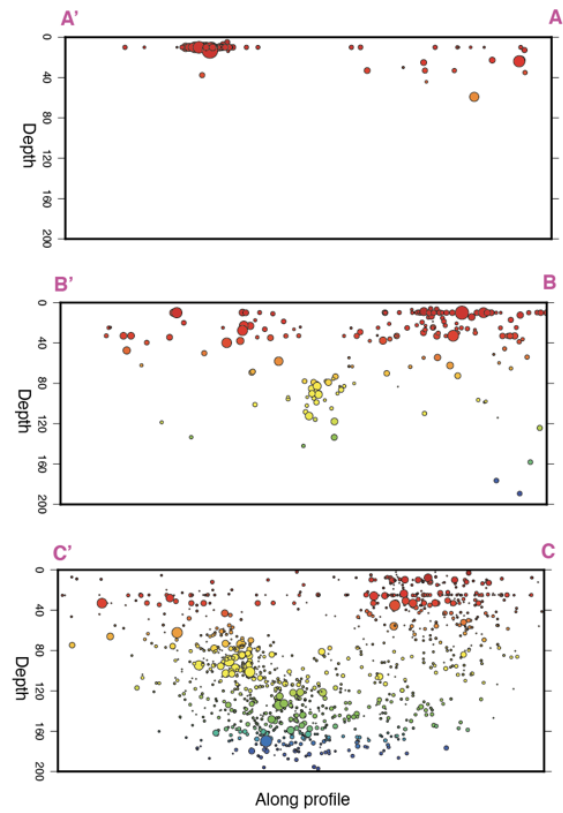
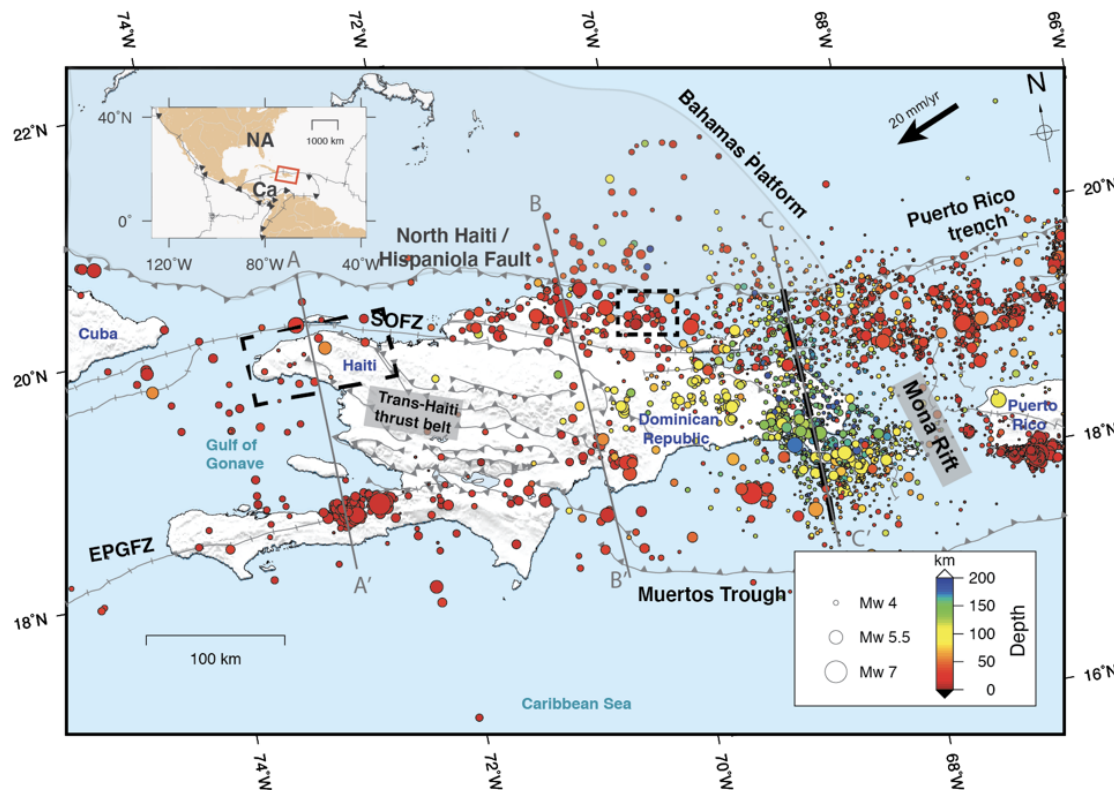


Figure S2. Fault traces used for modeling the 2021 Haiti earthquake, based on the CCAF-DB model. We extended the northern EPGFZ fault trace to connect with the southern trace for the modeling. (top) fault traces plotted on a satellite image of the region. (middle) Faults in the local coordinate system, numbered by segment. (bottom) 3D view of the faults, colored by dip.

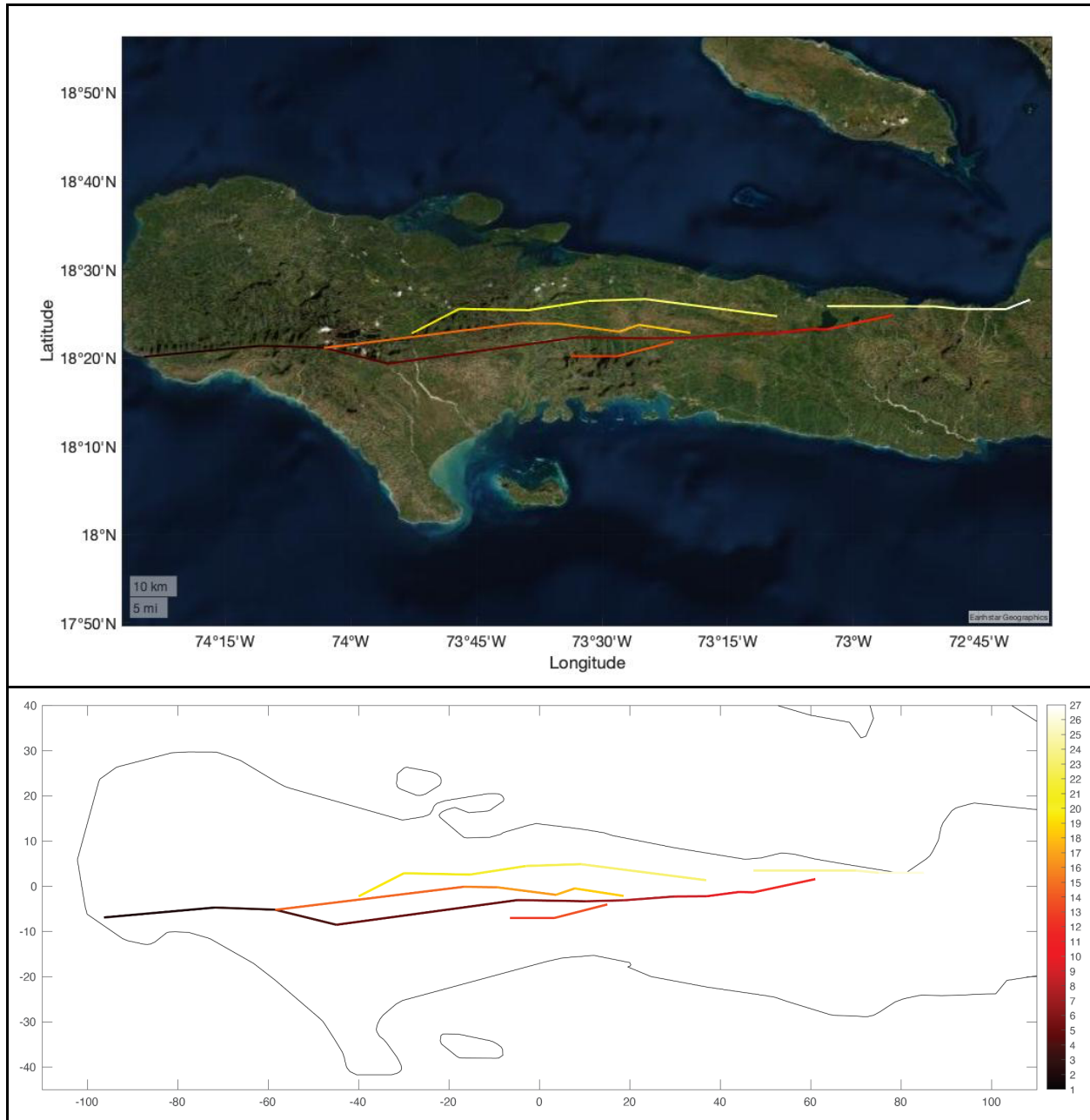


Figure S3. Preferred fault model geometry used for modeling the 2021 Haiti earthquake, based on the traces shown in Figure S3. (a) View from the southeast. ((b)) View from the northeast. (c) View from the south looking directly at the fault.

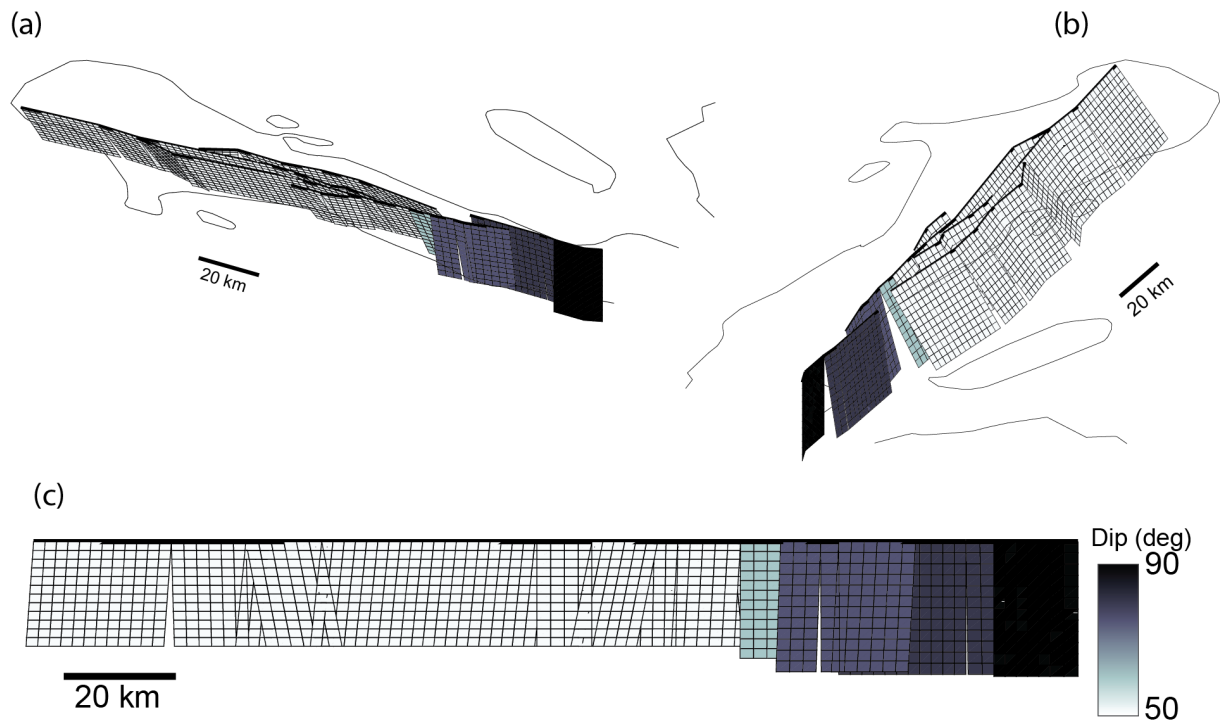


Figure S4. Original full-resolution InSAR and pixel offset displacements for Sentinel-1 and ALOS-2 used in this study.

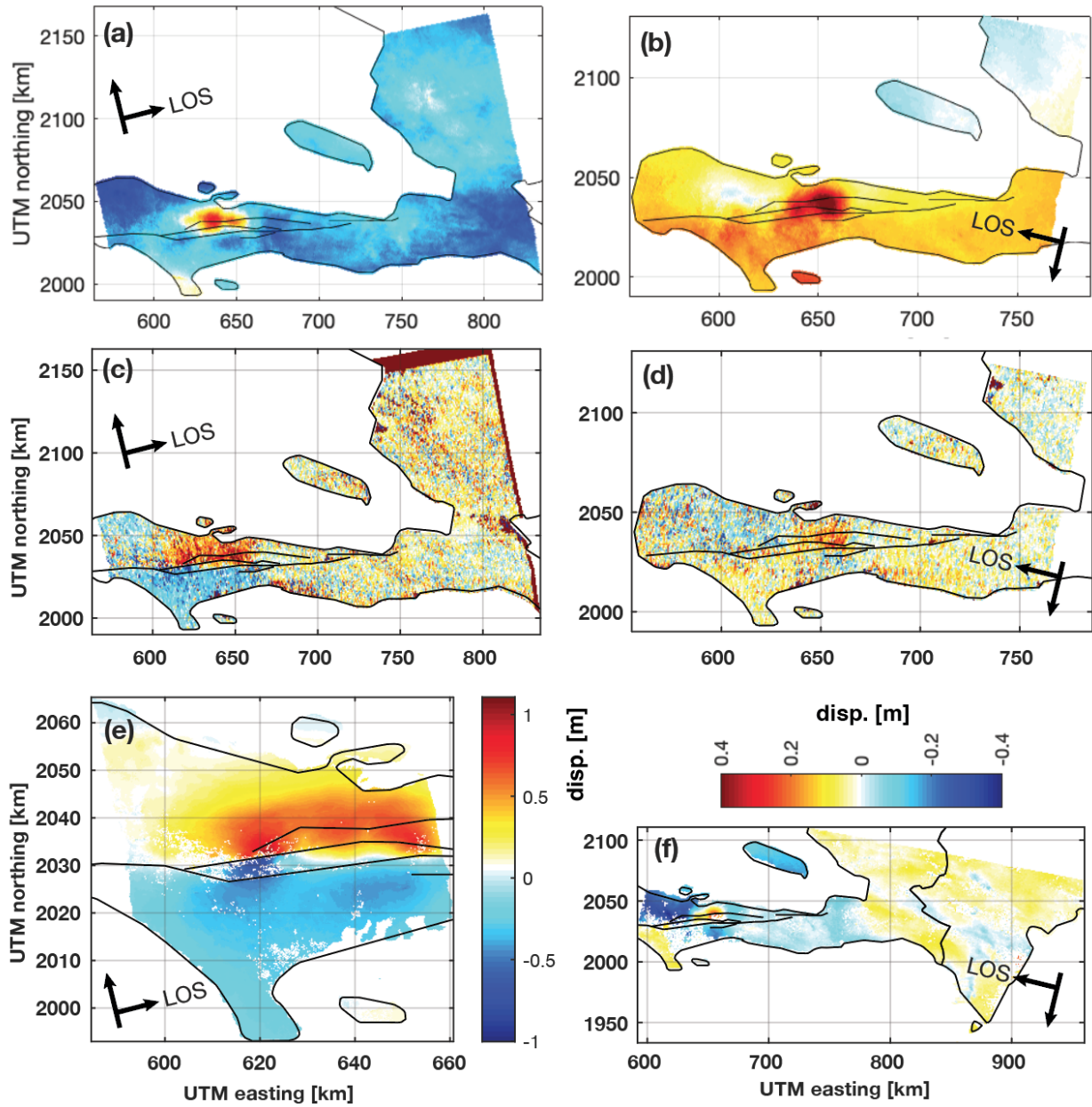


Figure S5. InSAR correlation and mask applied for Sentinel-1 track 4 and track 142 InSAR.

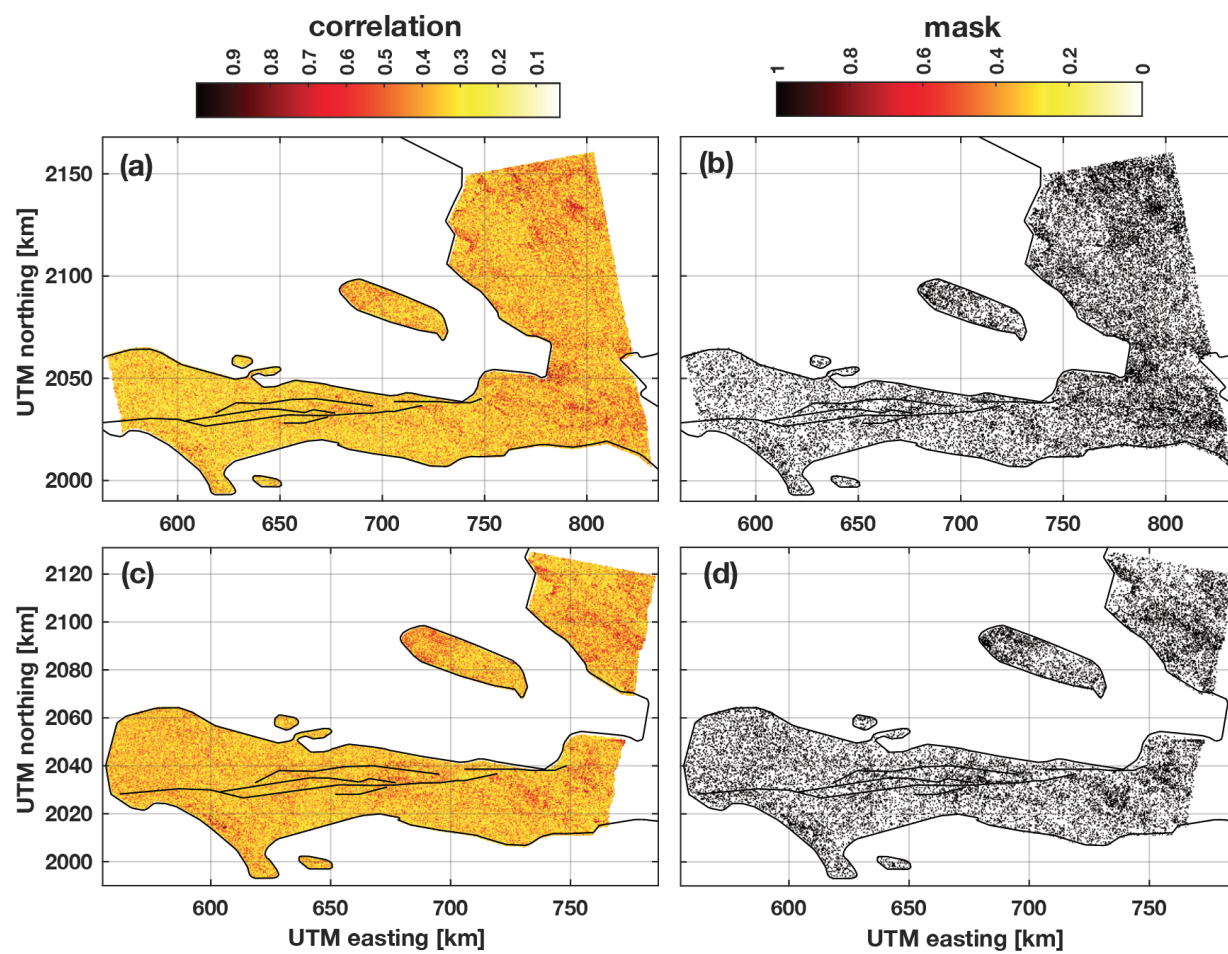


Figure S6. Covariance model used to generate data covariance matrix. (a-f) Full resolution displacements, noise region, covariance function and covariogram for Sentinel-1 ascending track 4 and descending track 142 interferograms. We estimate the covariance function using the undeformed region shown in (b,e). (g-l) Full resolution displacements, noise region, covariance function and covariogram for Sentinel-1 ascending track 4 and descending track 142 range pixel offsets. Directional covariance function estimated from undeformed region in shown in (h,k).

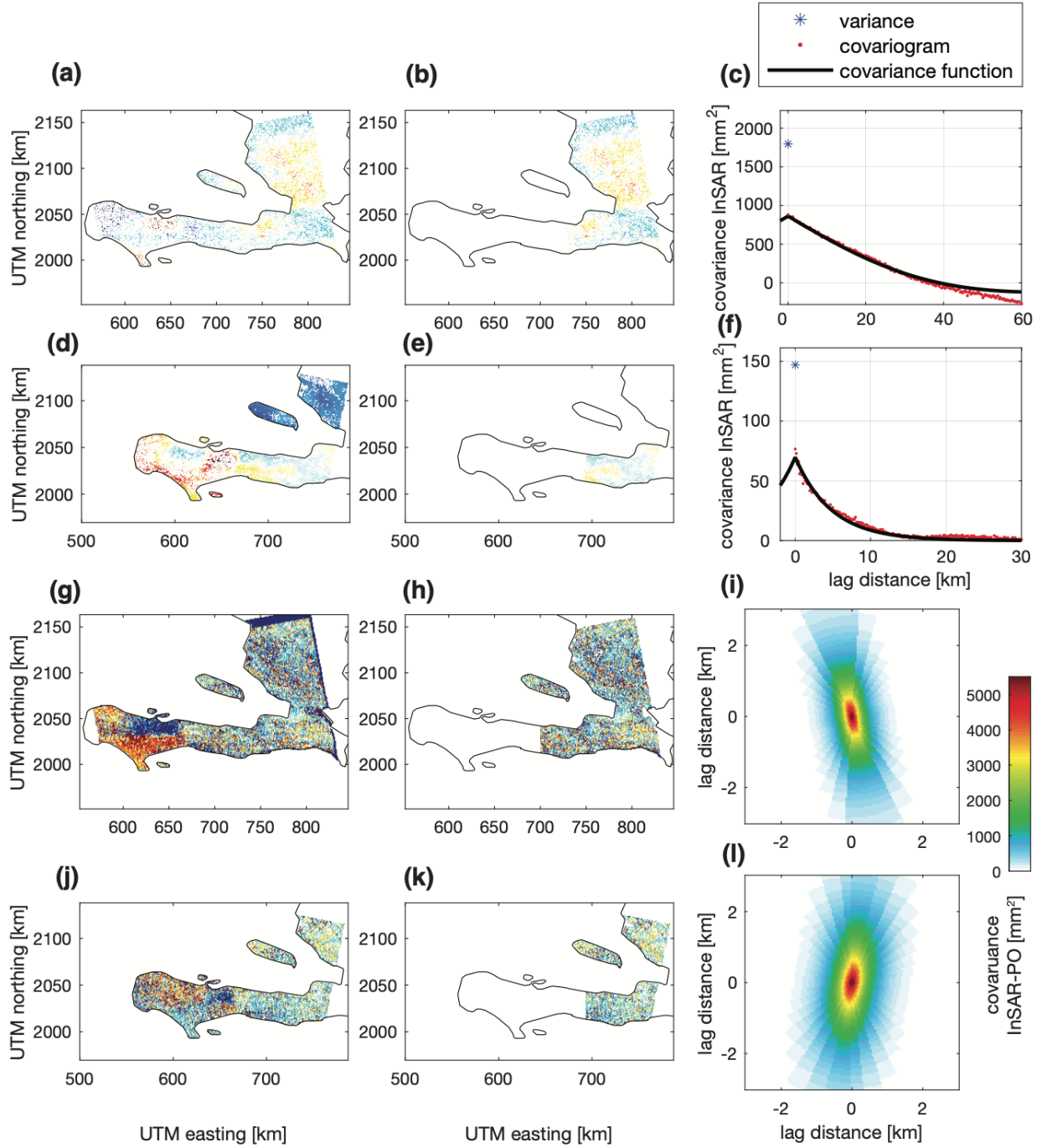


Figure S7. Data covariance matrices used in slip estimation. (a,b) correspond to that of Sentinel-1 ascending track 4 and descending track 142 interferograms, while (c,d) to that of range pixel offsets. (e,f) correspond to that of ALOS PALSAR-2 ascending track 43 and descending track 138 interferograms.

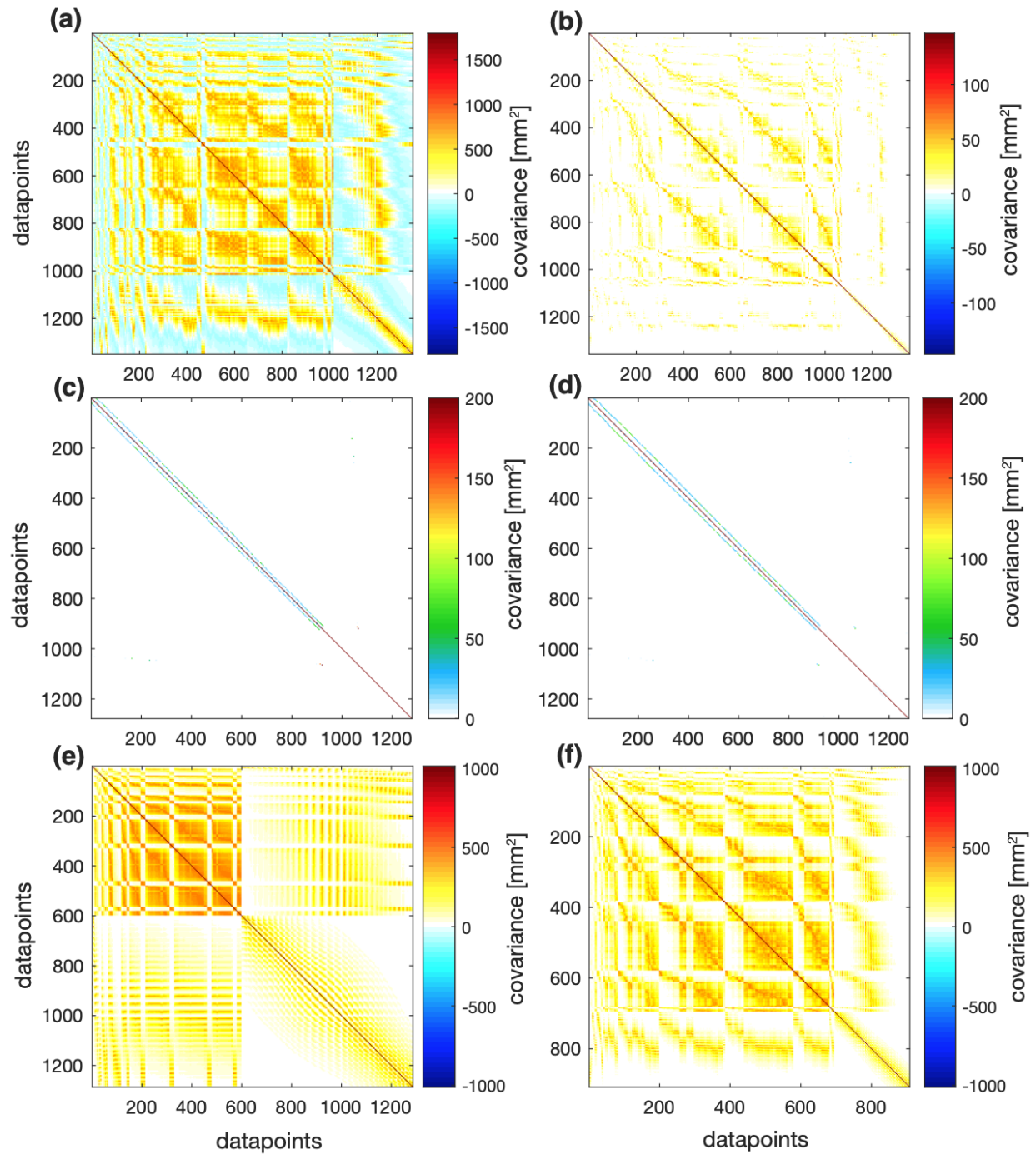
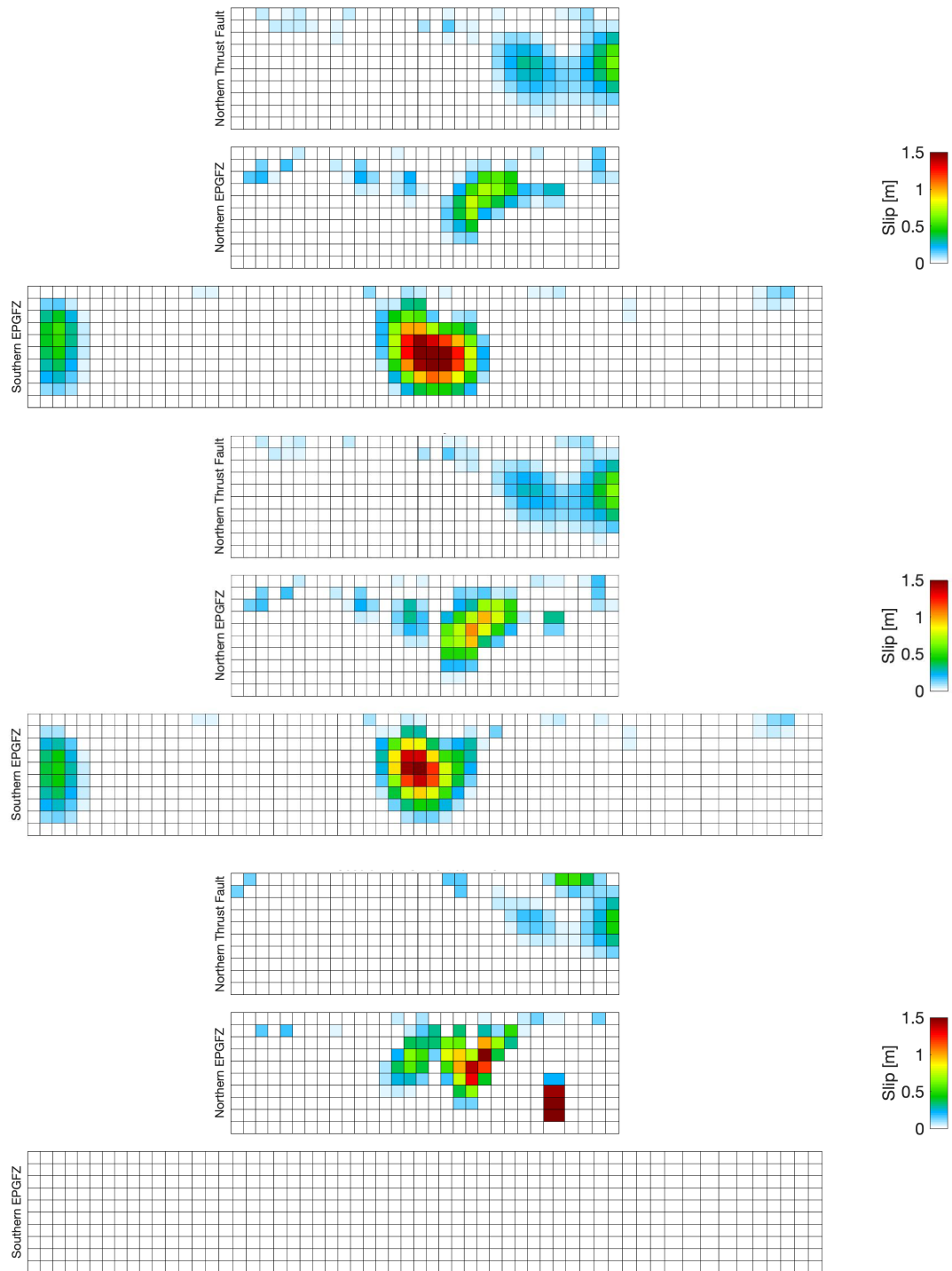


Figure S8. Estimated coseismic dip-slip in the preferred model compared to a model with steeper dip on the southern EPGFZ and a model with a south-dipping EPGFZ. (top) Preferred model (EPGFZ dipping 51 degrees). (second) EPGFZ dipping 70 degrees. (third) Vertical EPGFZ. (bottom) EPGFZ dipping 70 degrees south.



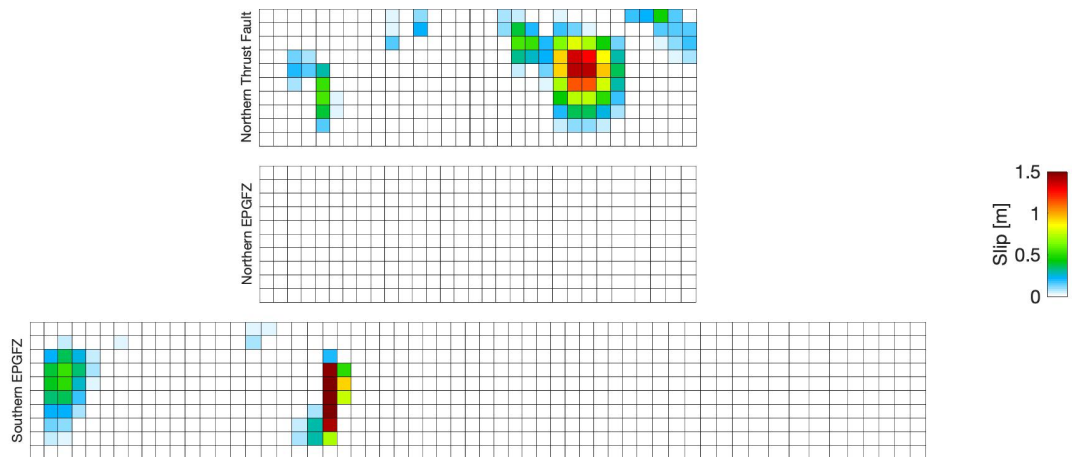
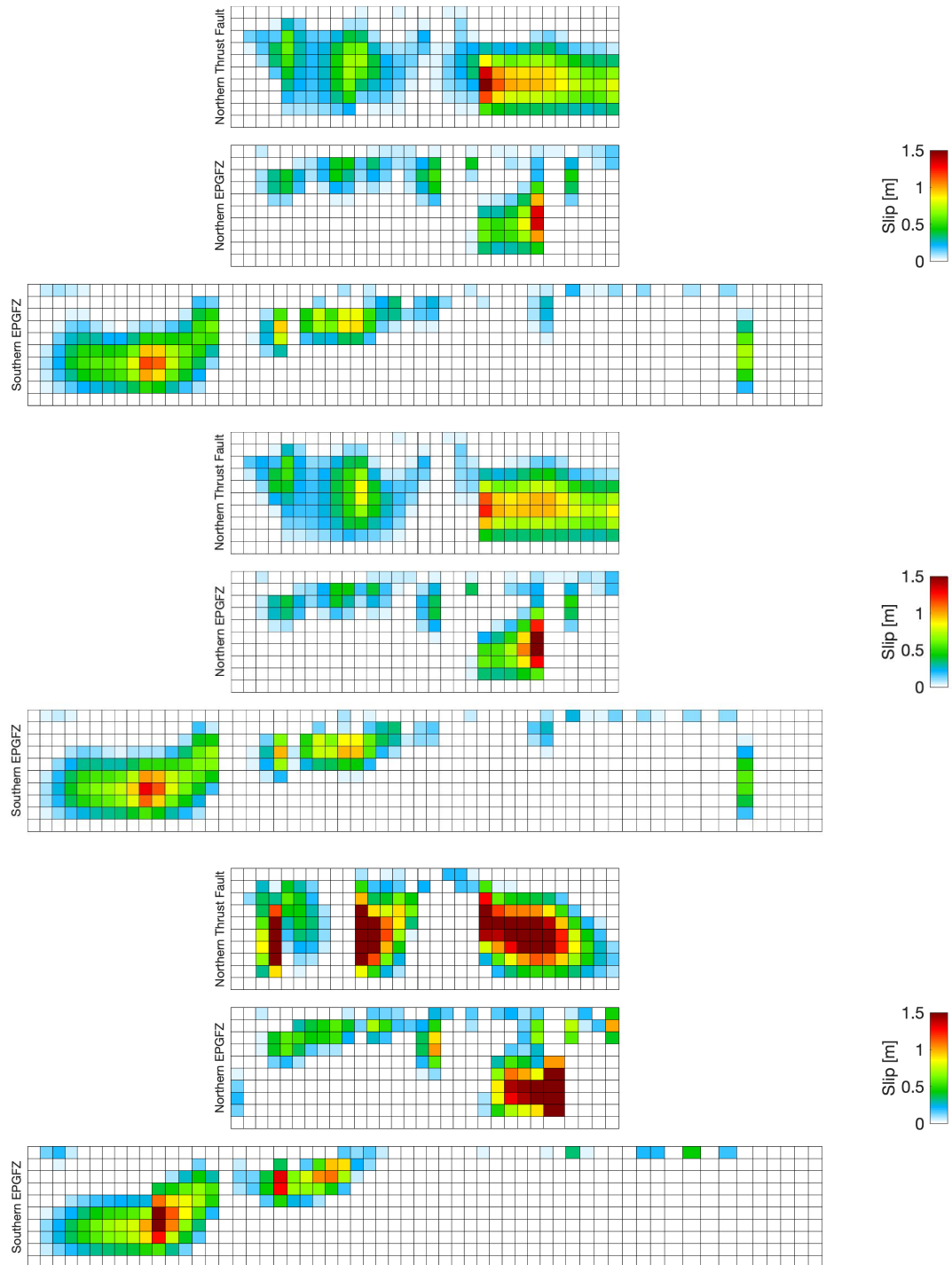


Figure S9. Estimated coseismic strike-slip in the preferred model (top) compared to a 70-degree dipping EPGFZ (second), vertical southern EPGFZ (third), and south-dipping EPGFZ (bottom).



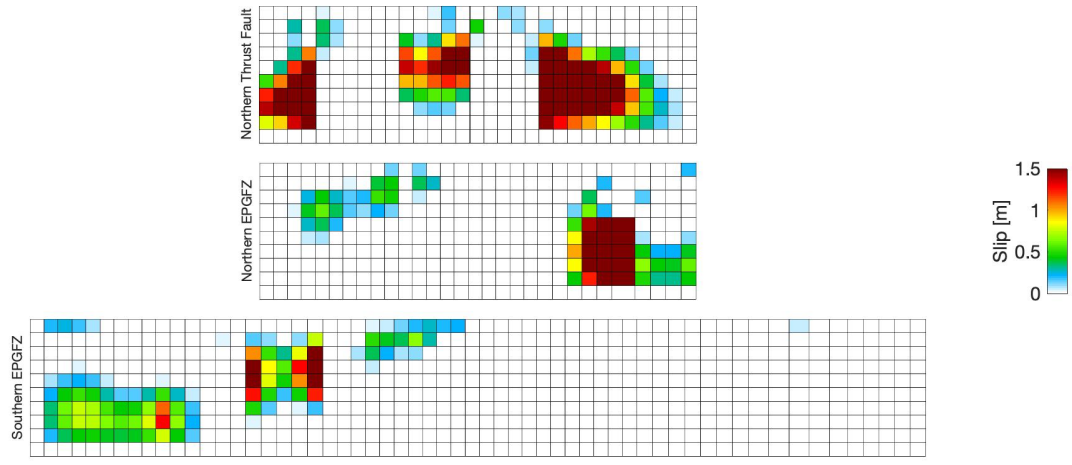


Figure S10. Coseismic slip in an EPGFZ-only model. In this model the fault dips 51 degrees north. (top) Reverse slip. (bottom) left-lateral slip.

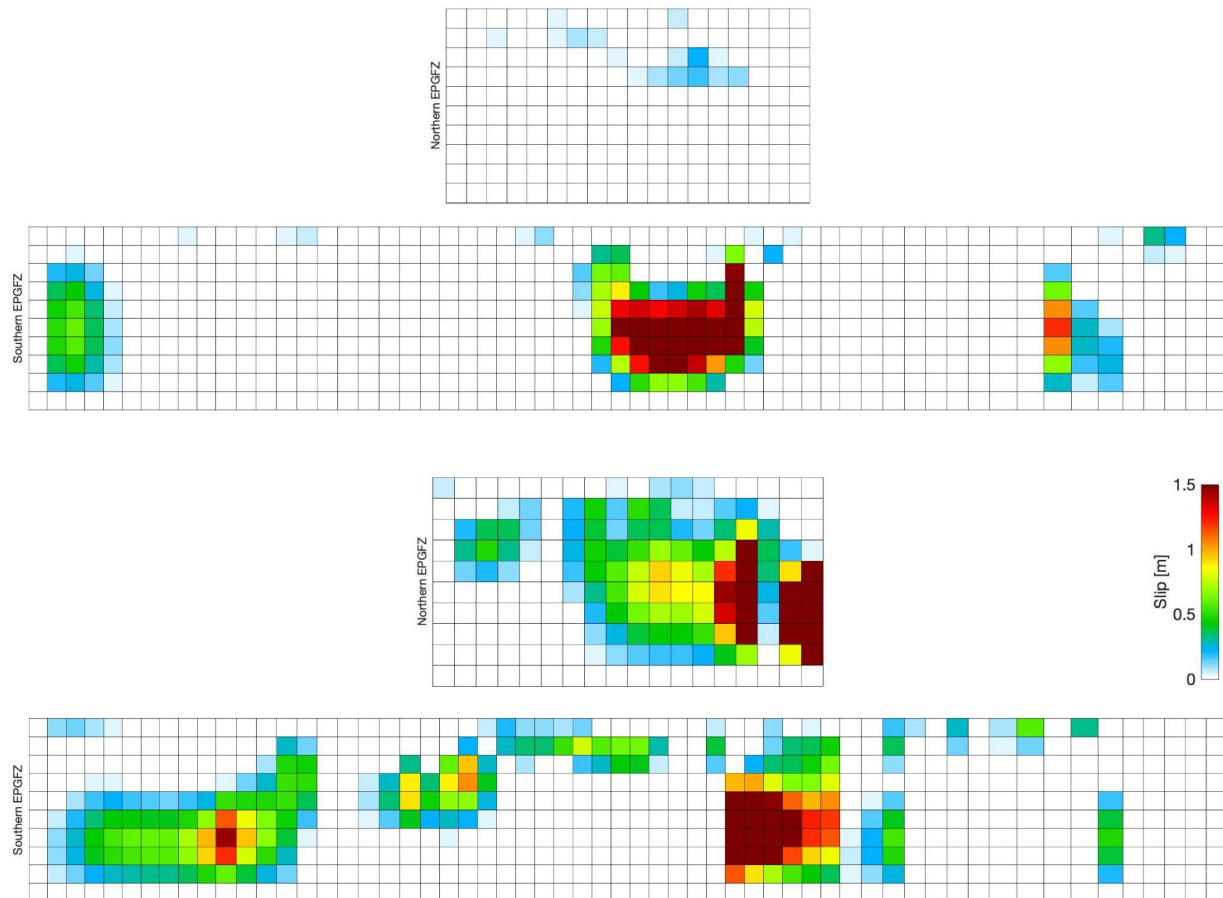


Figure S11. Misfits for the InSAR observations and pixel offsets for the preferred model (EPGFZ dipping 51 degrees). Local x and y are in units of km. Top row - Sentinel-1 InSAR. Middle row - Sentinel-1 SAR pixel offsets. Bottom row - ALOS-2 InSAR. Left column - Ascending data. Right column - Descending data.

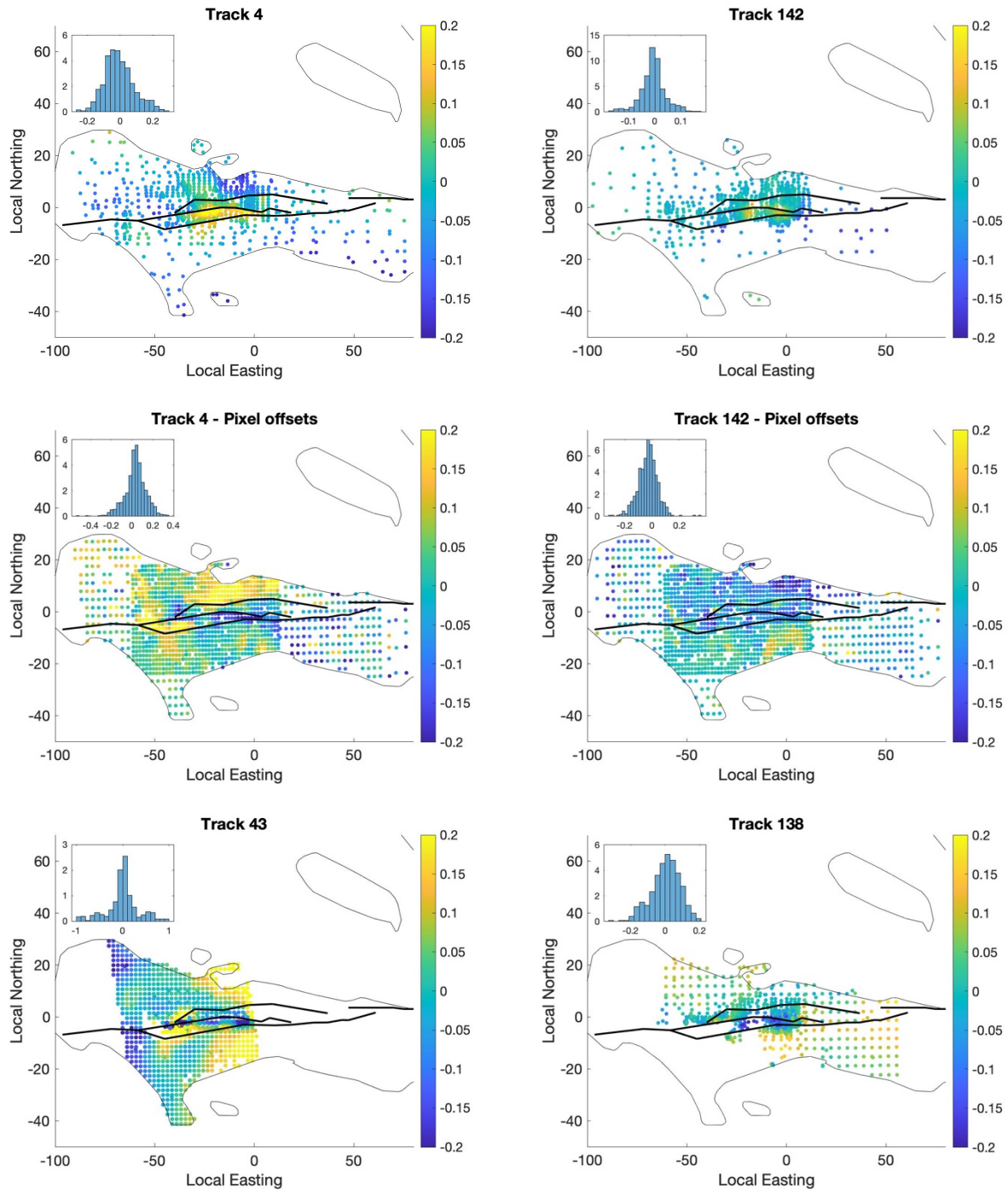


Figure S12. Misfits for the InSAR observations and pixel offsets assuming a vertical EPGFZ. Local x and y are in units of km. Top row - Sentinel-1 InSAR. Middle row - Sentinel-1 SAR pixel offsets. Bottom row - ALOS-2 InSAR. Left column - Ascending data. Right column - Descending data.

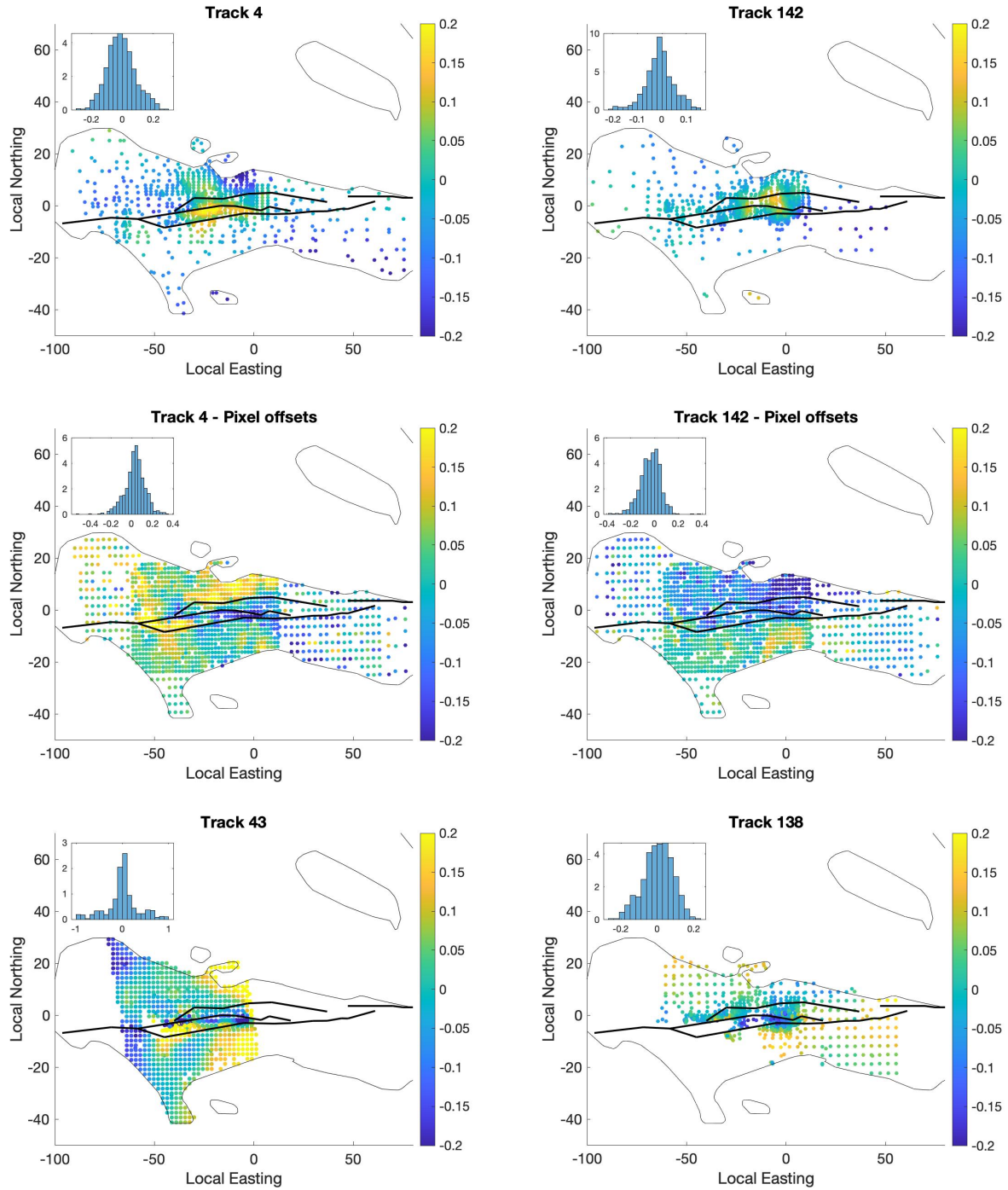


Figure S13. Residuals for the InSAR observations and pixel offsets assuming a south-dipping EPGFZ (70 degrees to the south). Local x and y are in units of km. Top row - Sentinel-1 InSAR. Middle row - Sentinel-1 SAR pixel offsets. Bottom row - ALOS-2 InSAR. Left column - Ascending data. Right column - Descending data.

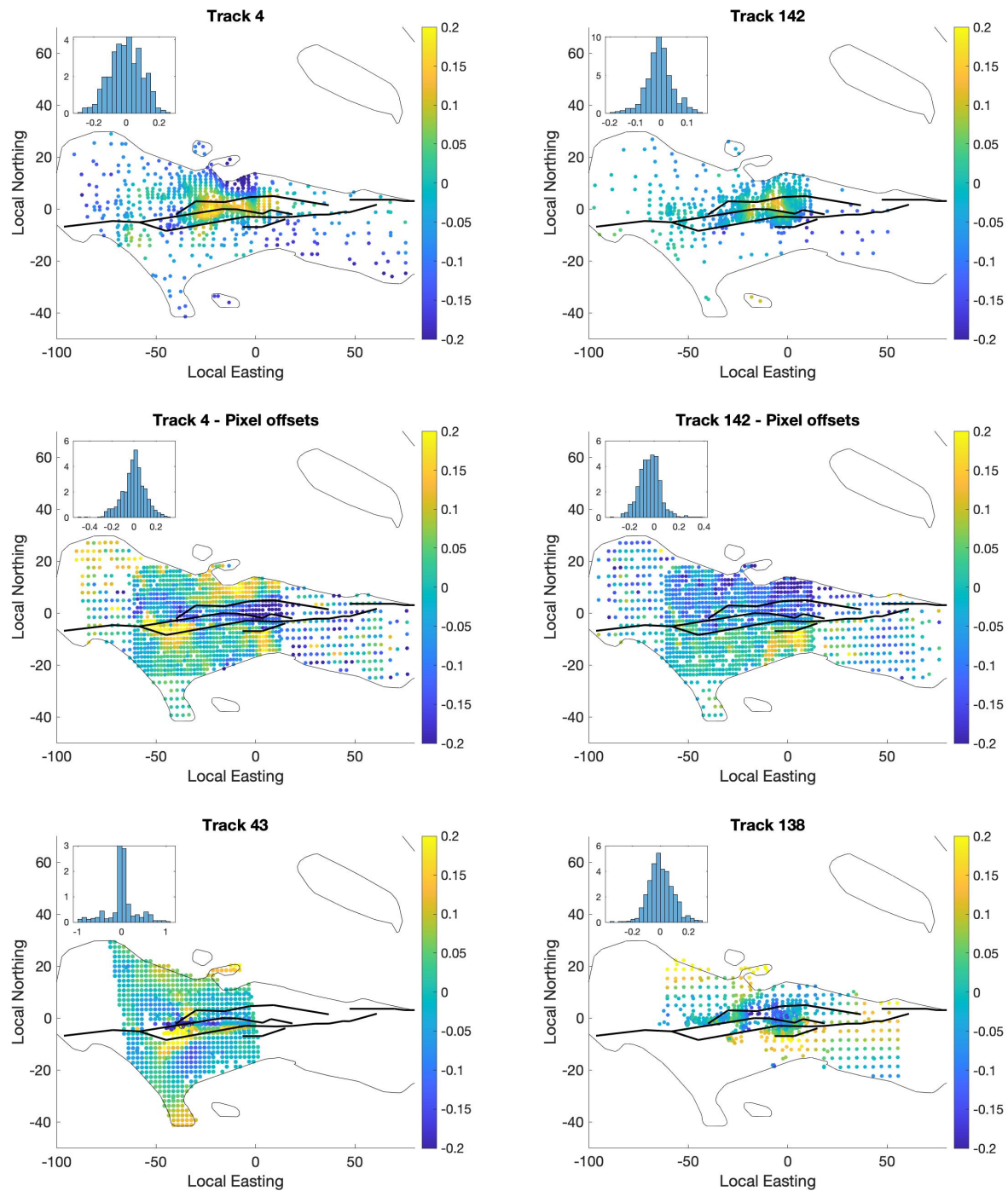


Figure S14. Misfits for the InSAR observations and pixel offsets for an EPGFZ-only model that includes both the northern and southern branches. Local x and y are in units of km. Top row - Sentinel-1 InSAR. Middle row - Sentinel-1 SAR pixel offsets. Bottom row - ALOS-2 InSAR. Left column - Ascending data. Right column - Descending data.

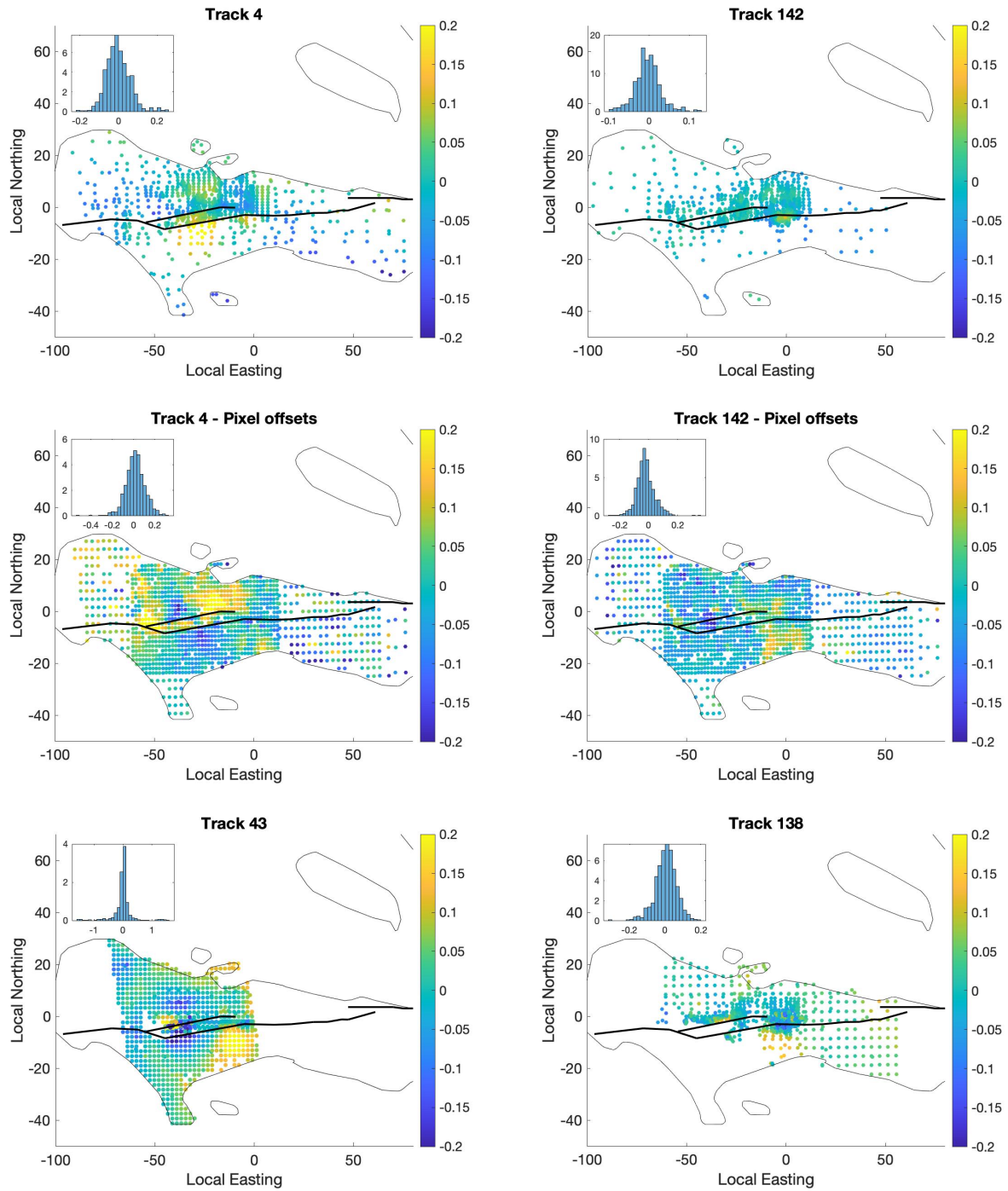


Figure S15. L-curve for model-norm regularization parameter. X-axis is the model norm of each solution, while the y-axis is the corresponding chi-squared misfit for that model. The minimum-curvature hyperparameter to be a scalar multiple of the minimum-norm parameter. Vertical lines show the parameter values for models shown in figures S16-S17. The smoothness parameter is fixed in each inversion.

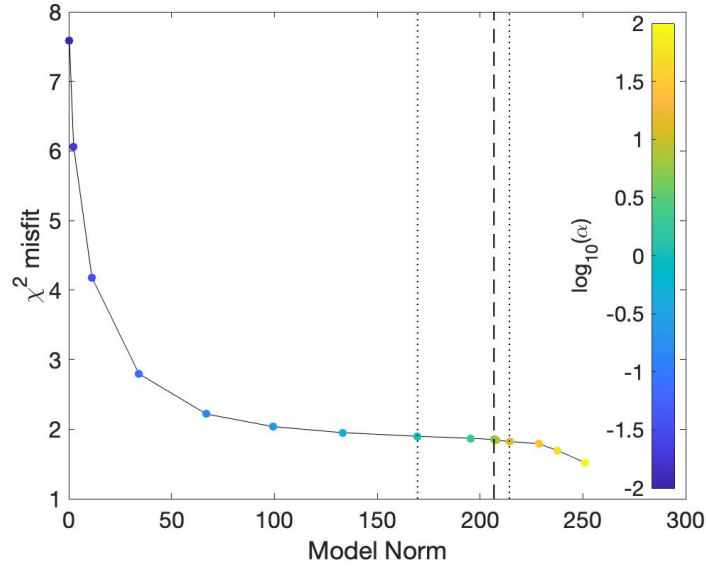


Figure S16. Estimated coseismic dip-slip in the preferred model (middle) compared to two models that have rougher slip (top) and smoother slip (bottom).

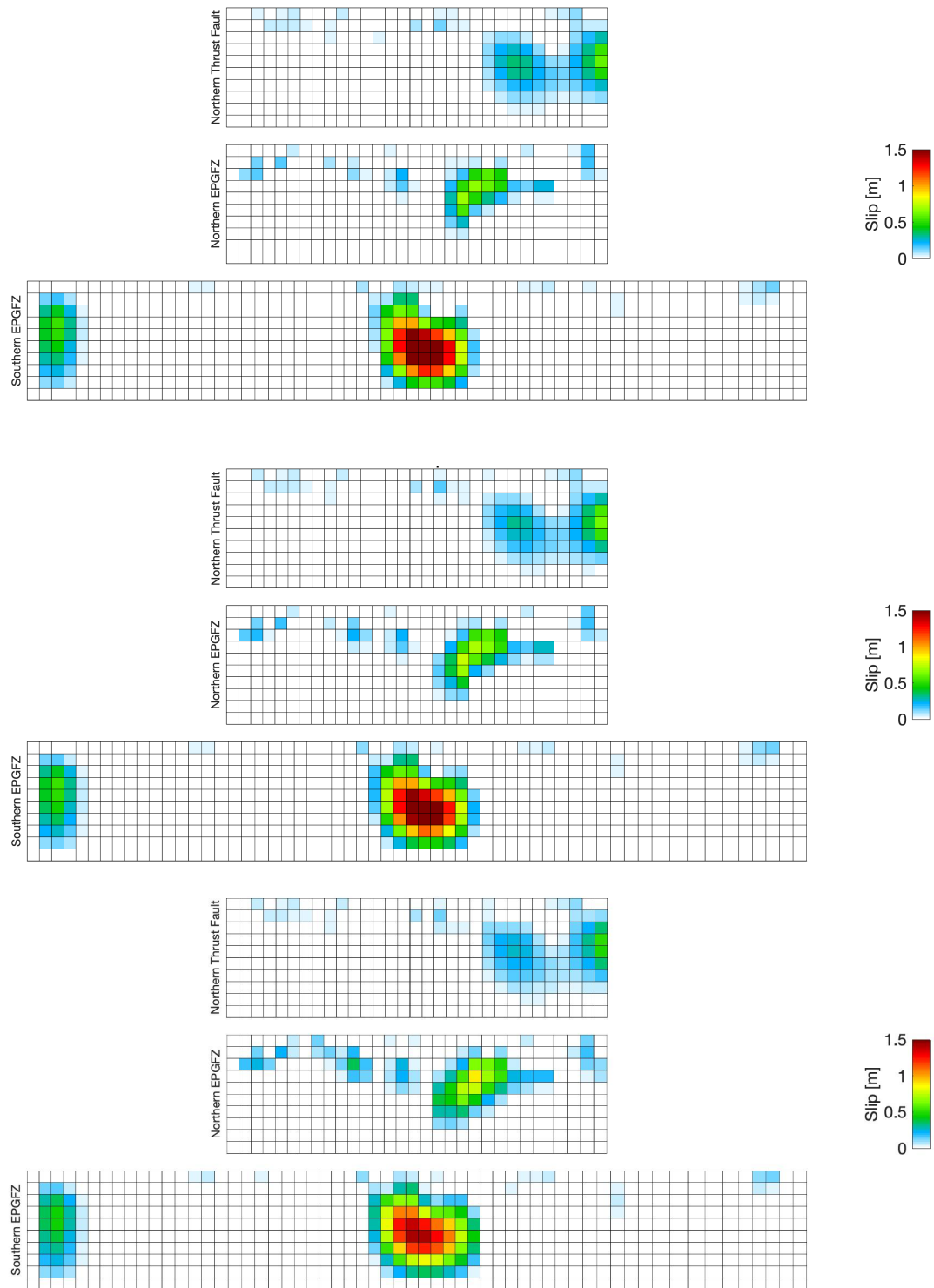


Figure S17. Estimated coseismic strike-slip in the preferred model (middle) compared to two models that have rougher slip (top) and smoother slip (bottom).

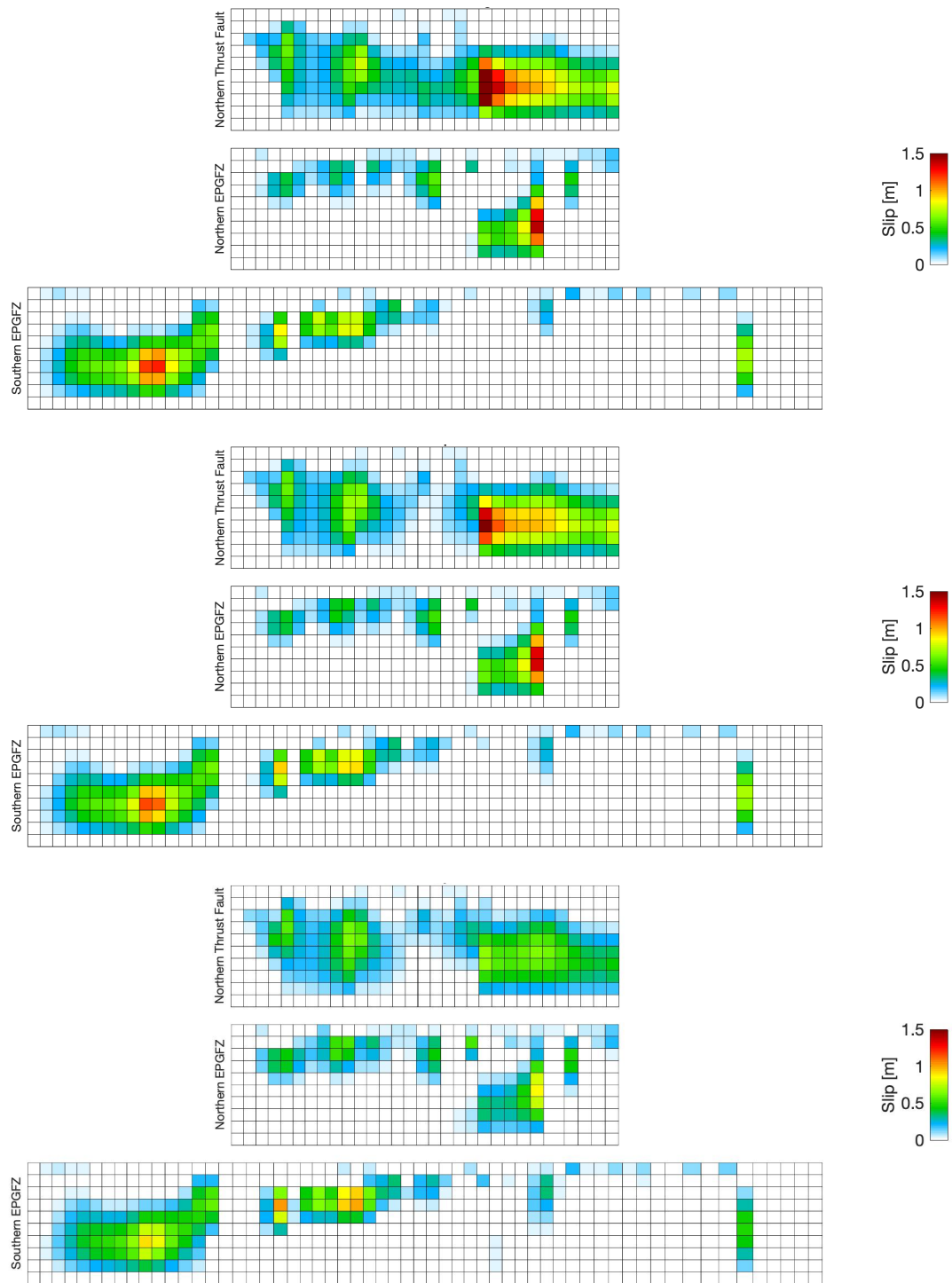
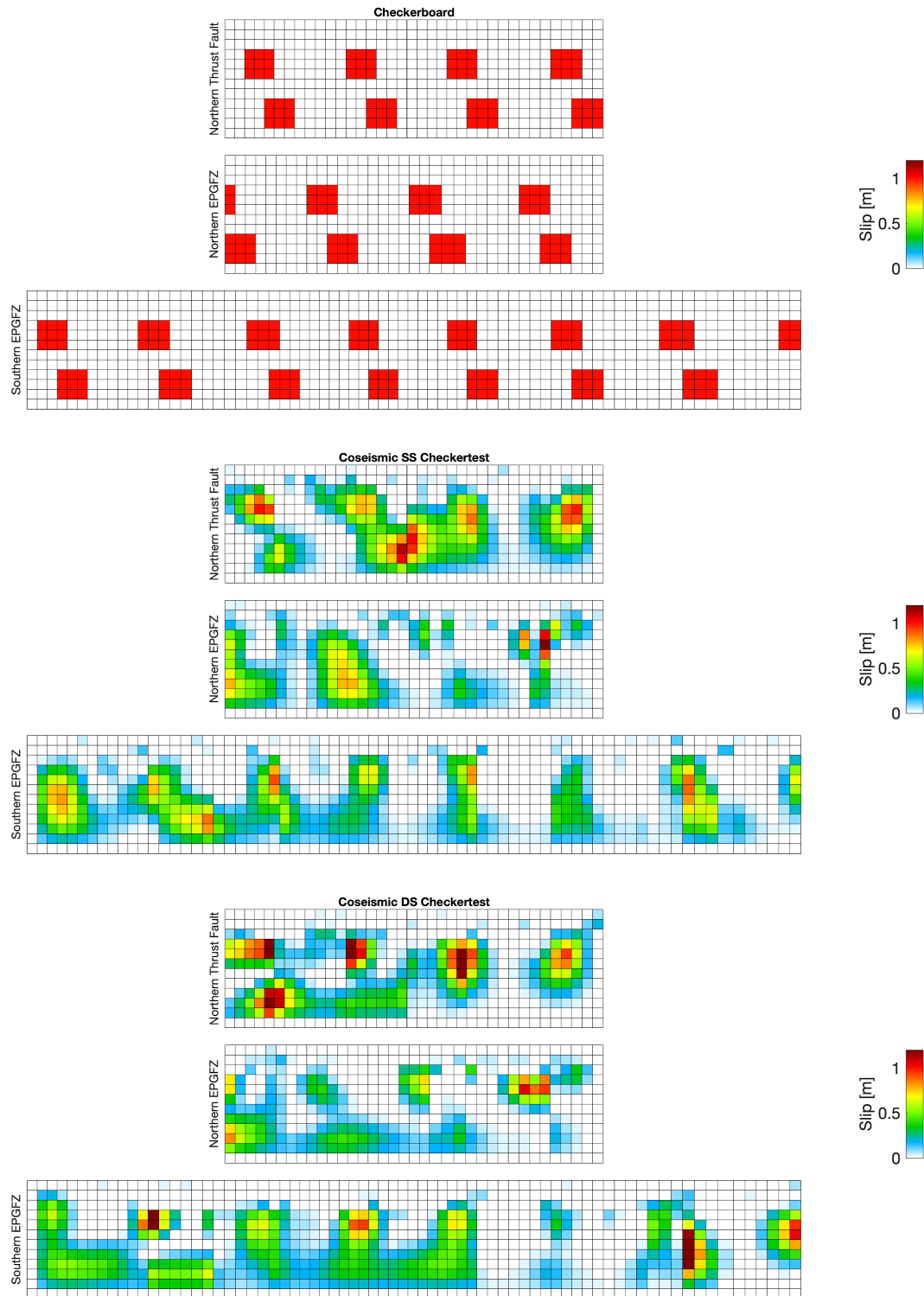
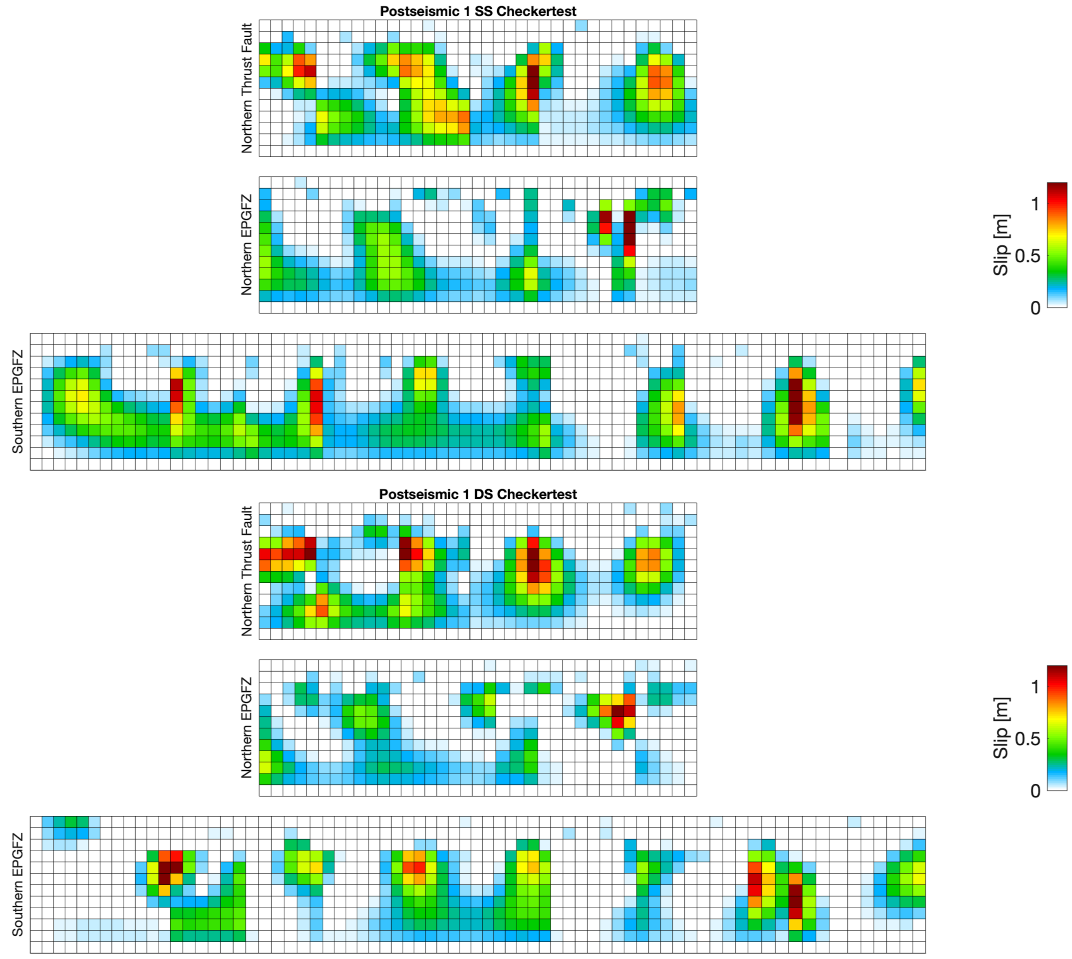


Figure S18. Results from a checkerboard test using all six datasets. The checkerboard pattern was the same for each time period (coseismic, postseismic 1, and postseismic 2) and each component (strike-slip and dip-slip).





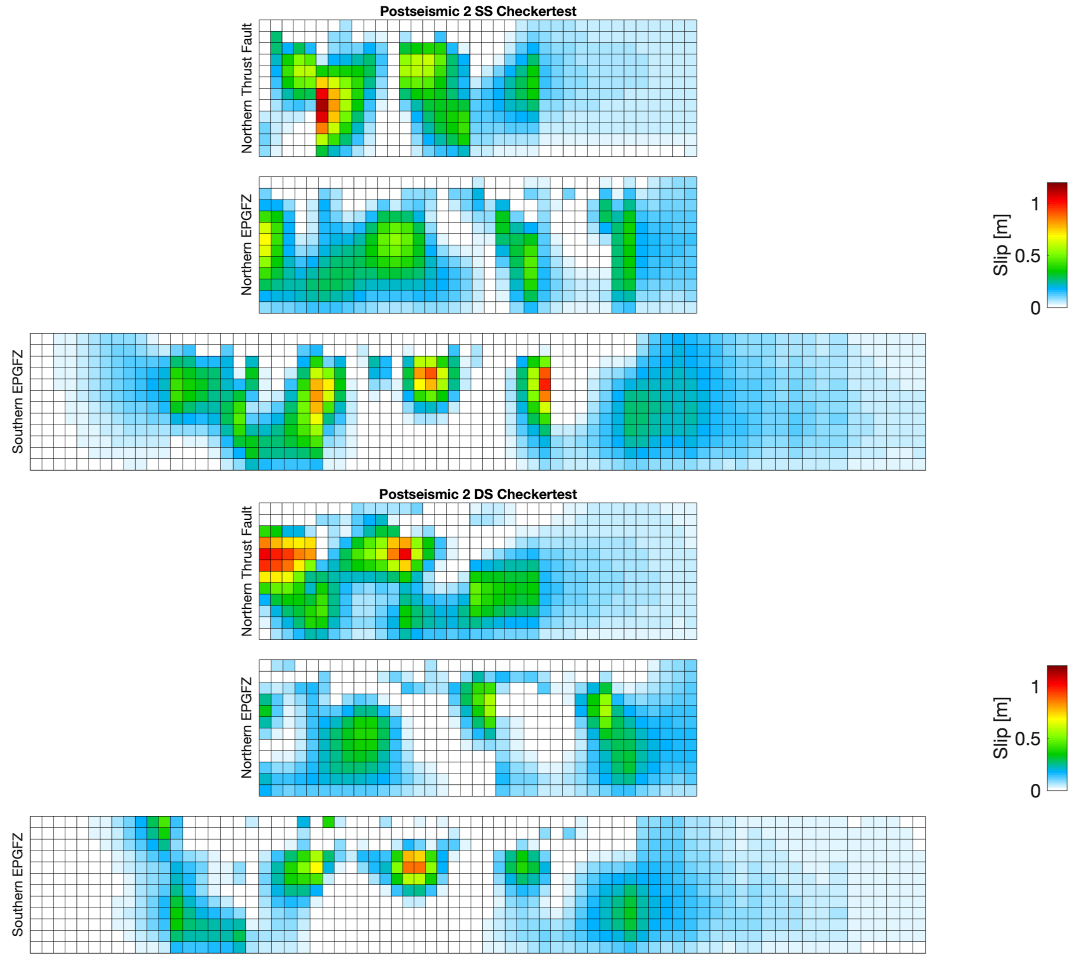
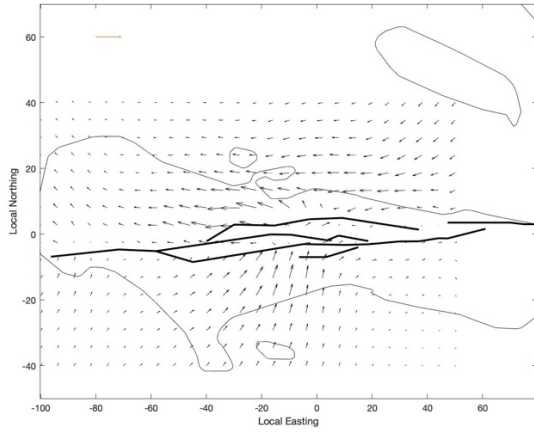
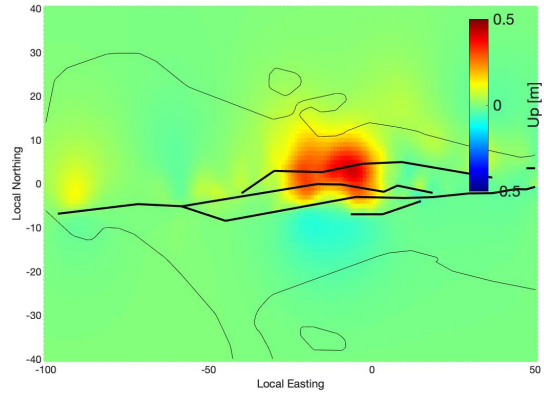


Figure S19. Predicted 3D displacements for the preferred model. Horizontal displacements are on the left, vertical on the right. (a-b) Coseismic displacements. (c-d) Displacements for the first postseismic phase. (e-f) Displacements for the second postseismic phase.

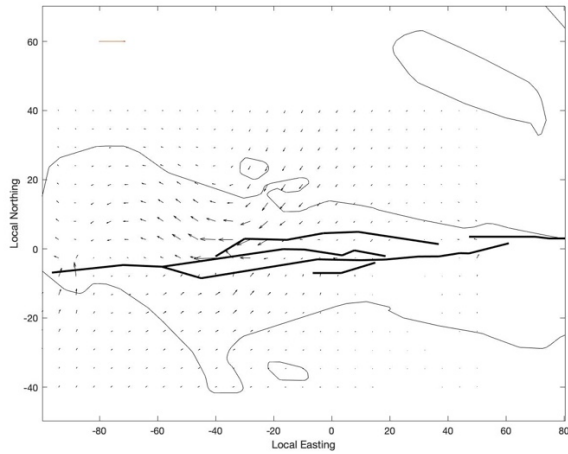
(a)



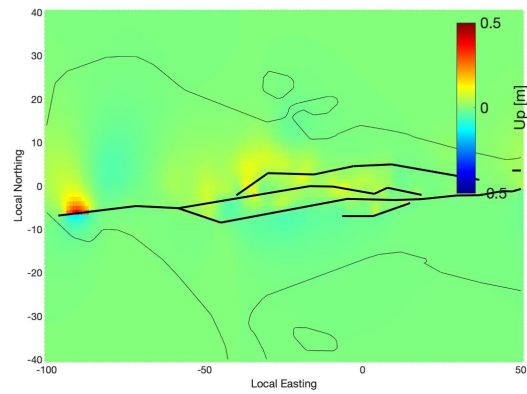
(b)



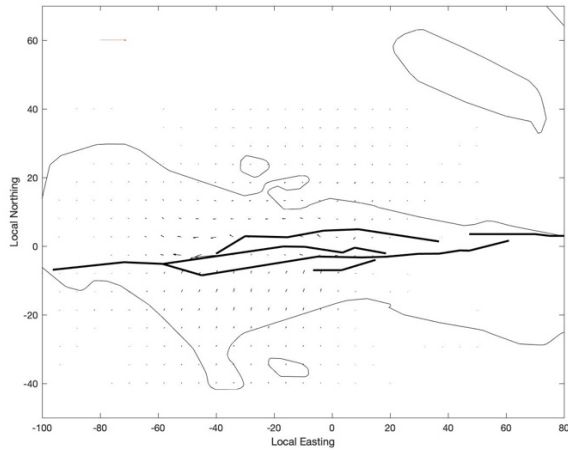
(c)



(d)



(e)



(f)

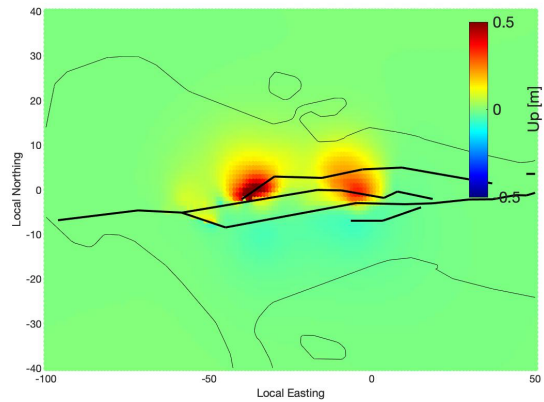
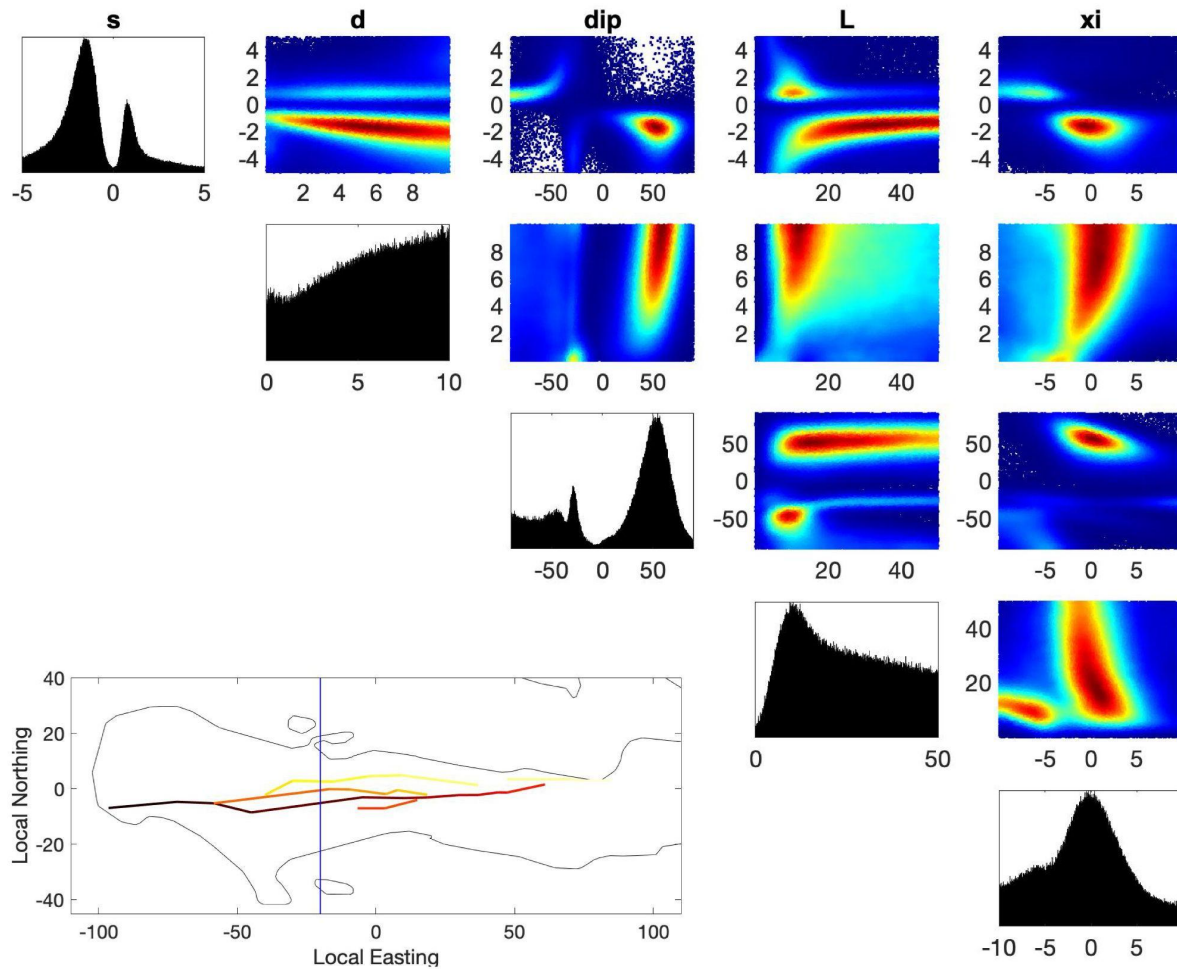
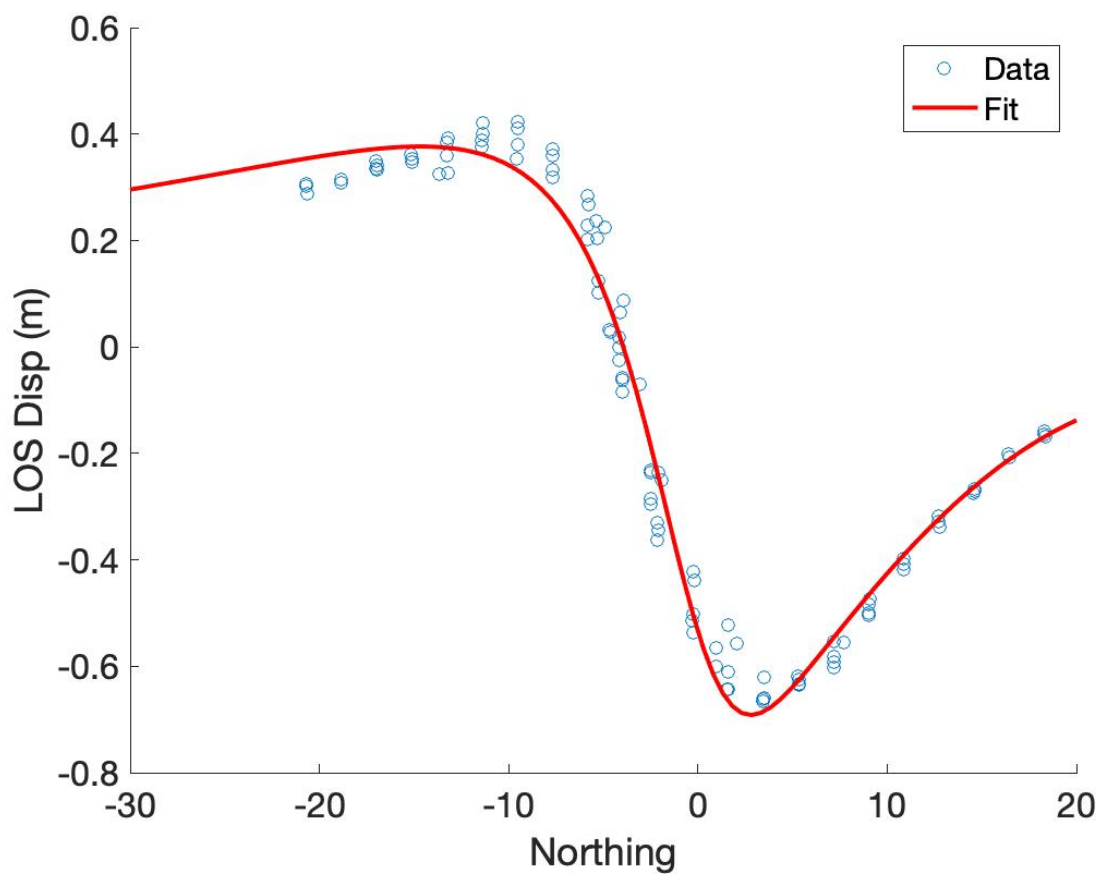


Figure S20. MCMC results for a single dipping plane-strain reverse fault using a profile of ALOS-2 track 43 across the hypocenter area. The profile is a line trending north-south at a location 20 km west of the origin. Data points are taken within 5 km of this line. (a) MCMC correlation plot showing the posterior probability density function for each parameter. Parameters are s : slip (m), d : depth of top of fault (km), dip : dip from horizontal in degrees, dip is to the north, L : fault length in km, and xi : Northing position of the top of the fault. Inset shows the profile location. (b) Data and maximum likelihood estimate (MLE) fit. Note that the LOS vector here points from the satellite to the ground, so negative displacements are motion towards the satellite.

(a)



(b)



Supplemental Tables

Table S1. Synthetic Aperture RADAR (SAR) Scenes Analyzed

Sensor	Track/Pass	Type / Frame	Date	Time (UTC)	SAR Timing
ALOS-2 PALSAR-2	138 / Desc	ScanSAR / -	2019/12/10	16:42	preseismic
ALOS-2 PALSAR-2	43 / Asc	Stripmap / -	2020/12/23	5:02	preseismic
Sentinel-1	142 / Desc	TopsScan / 530	2021/08/03	10:48	preseismic
Sentinel-1	4 / Asc	TopsScan / 55	2021/08/05	23:02	preseismic
Sentinel-1	142 / Desc	TopsScan / 530	2021/08/15	10:48	postseismic
ALOS-2 PALSAR-2	138 / Desc	ScanSAR / -	2021/08/17	16:42	postseismic
Sentinel-1	4 / Asc	TopsScan / 55	2021/08/17	23:02	postseismic
ALOS-2 PALSAR-2	43 / Asc	Stripmap / -	2021/08/18	5:02	postseismic

Table S2. Interferograms Analyzed

Sensor Track (Pass)	Dates (yyyy/mm/dd)	Processing	Range / Azimuth Looks	Bperp (m)
ALOS2 - 43 (Asc)	2020/12/23 - 2021/08/18	InSAR	-	8
ALOS2 - 138 (Desc)	2019/12/10 - 2021/08/17	InSAR	-	165
S1 - 4 (Asc)	2021/08/05 - 2021/08/17	InSAR	9 / 3	10.32
S1 - 142 (Desc)	2021/08/03 - 2021/08/15	InSAR	9 / 3	25
S1 - 4 (Asc)	2021/08/05 - 2021/08/17	SAR Pixel offsets	9 / 3	10.32

S1 - 142 (Asc)	2021/08/03 - 2021/08/15	SAR Pixel offsets	9 / 3	25
---------------------------	----------------------------	----------------------	-------	----

Table S3. Hyperparameters and individual dataset misfits from different inversion runs. The regularization parameter noted is the minimum-norm hyperparameter; the minimum-curvature parameter is 10% of that value.

Model Name	Hyper- parameter	A2- D138	A2- A43	S1- D142	S1- D142 pixel offset	S1- A4	S1- A4 pixel offset
Preferred, equal data weights	3.7276 / 0.1	2.53	32.09	1.99	0.74	1.24	0.89
Preferred, S1 downweighted	Same as above	2.32	31.9	0.51	0.66	0.40	0.89
Preferred, S1-po upweighted	Same as above	2.57	32.16	2.1	1.38	1.22	1.56
2 - EPGFZ 70 deg	Preferred	2.65	32.43	2.33	1.42	1.36	1.55
3 - EPGFZ 90 deg	Preferred	6.14	34.3	8.38	2.03	4.04	1.93
4 - South-dipping EPGFZ (65 deg)	Preferred	6.4	30.3	9.59	2.97	4.24	1.87
5 - Smooth slip	Alpha=1	2.57	34.00	2.12	1.41	1.75	1.70
	Alpha =						
6 - Rough slip	13.9	2.60	31.5	2.13	1.38	1.08	1.48
7 - EPGFZ only	Preferred	4.17	18.9	6.33	1.87	1.59	1.68

Table S4. Moment (magnitude equivalent), roughness norm, and overall (mean) misfit for each model.

Model Name	Hyper- parameter	Overall misfit	Roughness Norm	Coseismic Mw	Postseismic total Mw
Preferred, equal data weights	3.7276 / 0.1	2.02	5.08	7.07	7.03
S1 downweighted	Preferred	1.92	4.98	7.02	7.07

S1po upweighted	Preferred	2.1	5.24	7.06	7.02
2 - EPGFZ 70 deg	Preferred	2.13	4.88	7.07	7.02
3 - EPGFZ 90 deg	Preferred	2.85	8.84	7.10	7.30
4 - South-dipping EPGFZ (65 deg)	Preferred	2.6	20.9	7.24	7.5
5 - Smooth slip	Alpha =1	2.23	3.81	7.03	6.83
6 - Rough slip	Alpha = 13.9	2.06	5.84	7.07	7.16
7 - EPGFZ only	Preferred	2.22	7.46	7.10	7.29